ACS Catalysis

pubs.acs.org/acscatalysis

Research Article

Robust ω-Transaminases by Computational Stabilization of the Subunit Interface

Qinglong Meng, Nikolas Capra, Cyntia M. Palacio, Elisa Lanfranchi, Marleen Otzen, Luc Z. van Schie, Henriëtte J. Rozeboom, Andy-Mark W. H. Thunnissen, Hein J. Wijma, and Dick B. Janssen*

Cite This: ACS Catal. 2020, 10, 2915−2928

Read Online

ACCESS | Metrics & More | Article Recommendations | Supporting Information

ABSTRACT: Transaminases are attractive catalysts for the production of enantiopure amines. However, the poor stability of these enzymes often limits their application in biocatalysis. Here, we used a framework for enzyme stability engineering by computational library design (FRESCO) to stabilize the homodimeric PLP fold type I ω-transaminase from *Pseudomonas jessenii*. A large number of surface-located point mutations and mutations predicted to stabilize the subunit interface were examined. Experimental screening revealed that 10 surface mutations out of 172 tested were indeed stabilizing (6% success), whereas testing 34 interface mutations gave 19 hits (56% success). Both the extent of stabilization and the spatial distribution of stabilizing mutations showed that the subunit interface was critical for stability. After mutations were combined, 2 very stable variants with 4 and 6 mutations were obtained, which in comparison to wild type (T_m^{app} = 62 °C) displayed T_m^{app} values of 80 and 85 °C, respectively. These two variants were also 5-fold more active at their optimum temperatures and tolerated high concentrations of isopropylamine and cosolvents. This allowed conversion of 100 mM acetophenone to (*S*)-1-phenylethylamine (>99% enantiomeric excess) with high yield (92%, in comparison to 24% with the wild-type transaminase). Crystal structures mostly confirmed the expected structural changes and revealed that the most stabilizing mutation, I154V, featured a rarely described stabilization mechanism: namely, removal of steric strain. The results show that computational interface redesign can be a rapid and powerful strategy for transaminase stabilization.

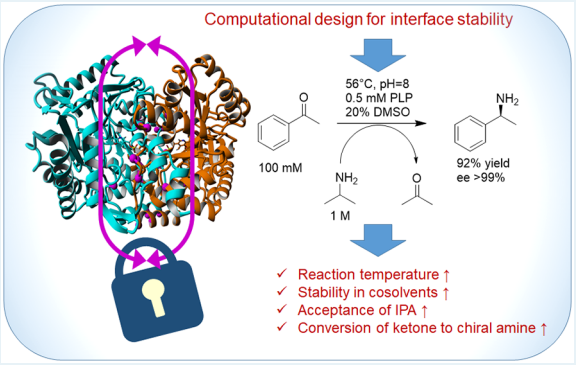

KEYWORDS: *transaminase, biocatalysis, computational design, thermostability, protein engineering, subunit interface*

INTRODUCTION

ω-Transaminases (ω-TAs) and amine transaminases (ATAs) are highly attractive biocatalysts to synthesize optically pure chiral amines, which are important intermediates in the synthesis of pharmaceuticals and other fine chemicals.[1−3] In the transaminase (TA) reaction, the pyridoxal 5′-phosphate (PLP) cofactor of the enzyme serves as a molecular shuttle to transfer an amino group from a donor (usually an amine or amino acid) to an acceptor (a ketone, aldehyde, or keto acid) (Scheme 1). The overall reaction consists of two parts, each involving several chemical steps.[4] In the first half-reaction the conserved lysine that forms a Schiff base with the PLP cofactor in the native protein (internal aldimine, E-PLP) is displaced by the amino donor. This gives an external aldimine, and via subsequent quinonoid and ketimine intermediates the amino group of the donor is transferred to the PLP, yielding the aminated pyridoxamine 5′-phosphate (PMP)−enzyme intermediate (E:PMP). The deaminated donor is released as a ketone, aldehyde, or keto acid. After this, in the second half-reaction, the amino acceptor binds and reacts with the E:PMP intermediate to form a ketimine, which subsequently

Scheme 1. Isopropylamine-Driven Transamination Reaction

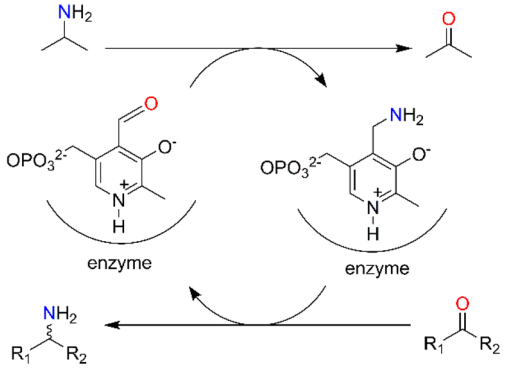

Received: December 3, 2019
Revised: January 31, 2020
Published: January 31, 2020

https://dx.doi.org/10.1021/acscatal.9b05223
ACS Catal. 2020, 10, 2915−2928

decomposes via a quinonoid and an external aldimine. Finally, the enzyme's lysine replaces the aminated acceptor, which is released, and the E:PLP enzyme is re-formed.

TAs can also convert prochiral ketones or keto acids to the corresponding amines with the nitrogen on a chiral carbon atom. This enables the production of enantiopure compounds by asymmetric catalysis if the reaction proceeds fast enough with high product enantioselectivity. This requires not only high enzyme activity but also enzyme robustness. Bioprocess conditions that should be tolerated include high reactant concentrations, the presence of cosolvents to increase reactant solubility, high temperature to accelerate reaction rates, and general stability to enable enzyme reuse.[5] Thus, to make TAs more suitable for application, improving enzyme stability is of key importance.[6]

Many of the TAs with attractive activities for synthetic applications are grouped as class III TAs in the PLP fold-type I family of enzymes.[7] These mostly dimeric enzymes are composed of identical subunits, and residues from both subunits contribute to the identical active sites. The stability of an enzyme of this class was recently improved by engineering cofactor binding,[8] on the basis of the notion that the aminated form of the cofactor PMP may be lost from the enzyme active site, followed by irreversible denaturation.[9,10] As in other enzymes, subunit dissociation may occur during inactivation.[11] It likely triggers local unfolding and exposure of hydrophobic patches which can aggregate, causing irreversible loss of activity. Furthermore, subunit dissociation could expose the hydrophilic PMP intermediate to solvent, causing cofactor loss. This suggests that strengthening intersubunit interactions may be used as a way to obtain more stable TAs. In agreement with these observations, we were not very successful with initial attempts to stabilize the TA used in this report by substituting surface-located residues in flexible regions identified by molecular dynamics simulations.

To test the hypothesis that interface mutations might stabilize TA, we investigated the recently described class III ω-TA from *Pseudomonas jessenii* (*Pj*TA), which exhibits low stability even during storage at room temperature, and we compared the effect of surface-located mutations to mutations at the subunits interface. *Pj*TA is a homodimeric PLP fold-type I enzyme with subunits of 456 amino acids.[12] The enzyme catalyzes the deamination of 6-aminohexanoate, which is the first intermediate in the bacterial degradation of the industrial nylon precursor caprolactam. The structures of the apoenzyme, external aldimine with 6-aminohexanoate, and PMP-bound enzyme were solved by protein crystallography.[12]

In recent years, the power of structure-based enzyme engineering has grown significantly due to the development of computer algorithms that can quantitatively predict the stability effects of mutations and designed sequences.[13−16] Using appropriate scoring functions, amino acid rotamer libraries, and search algorithms to find low-energy solutions, computational tools can search for potentially stabilizing mutations within the vast sequence space accessible by random mutagenesis.[17] For example, energy calculations with the RosettaDesign program were used to identify three variants of yeast cytosine deaminase, the apparent melting temperature (T_m^{app}) of which was increased by 10 °C.[18] Another approach focused on computational optimization of charge−charge interactions on the protein surface, and this method was successfully applied to increase the T_m^{app} of acylphosphatase and of Cdc42 GTPase by 10 °C.[19,20] Lee et al. increased stability of β-glucosidase A by 16 °C in T_m^{app} by the computational design of salt bridges.[21] Positions for a disulfide bond were identified by MD simulation to improve the stability of haloalkane dehalogenase.[22] A combination of phylogenetic analysis for enzyme stabilization, usually called the consensus approach,[23−25] and computational methods was reported by Bednar et al. (FireProt)[26] and Goldenzweig et al. (PROSS).[27] In this way, the thermostability of a dehalogenase was increased by 24 °C.[26] Stabilization of tetrameric glucose dehydrogenases by toward-consensus mutations at subunit interfaces was reported by Vázquez-Figueroa et al.,[28] in one case enhancing T_m^{app} by up to 35 °C, although most mutations had a small effect. Interface optimization through sequential rounds of rational design was described by Bosshart et al.,[29] increasing unfolding temperature of a homodimeric D-tagatose 3-epimerase by 23 °C.

Our group has explored a computational workflow called FRESCO (framework for rapid enzyme stabilization by computational libraries).[30] Briefly, a large number of potentially stabilizing mutations is predicted by folding energy calculations and then all possible point mutations are filtered by high-throughput molecular dynamics (MD) simulations and visual inspection to construct a small library. Verified mutations are combined, giving large increases in stability. This strategy has been applied to several enzymes:[30−37] e.g., the T_m^{app} of a monomeric haloalkane dehalogenase and a peptide amidase was increased by 23 °C with a 10% success rate among the tested mutations.[31,32]

In this report, we examined the use of the FRESCO workflow to improve the stability of *Pj*TA. In view of the dimeric structure and role of the PLP cofactor, we paid special attention to mutations at the subunit interface, as stabilization of multimeric enzymes may be achieved by preventing dissociation.[11,28,29] In combination with phylogenetic data, we predicted and experimentally confirmed multiple stabilizing mutations, mostly at the interface, which were combined to obtain two robust variants. The stabilized *Pj*TAs showed higher activity at their new higher temperature optima, enhanced cosolvent compatibility, and better isopropylamine (IPA)-driven conversion of acetophenone to (*S*)-1-phenylethylamine ((*S*)-1-PEA). The structural basis of the enhanced stability was revealed by protein crystallography.

MATERIALS AND METHODS

Materials. The chemicals sodium pyruvate, (*S*)-1-PEA, and IPA were purchased from Sigma-Aldrich. Acetophenone was obtained from Acros Organics. PLP was purchased from Fisher Scientific. The stain SYPRO Orange was purchased from Life Technologies. Other chemicals were of analytical grade purity.

Computational Design of Stabilizing Mutations. To design potentially stabilizing mutations in *Pj*TA, we followed the FRESCO protocol.[30,37] First, we calculated the effects on free energy of folding ($\Delta\Delta G^{fold}$) for point mutations at all positions in the protein, substituting with all proteinogenic amino acids except cysteine. The X-ray structures used were *Pj*TA-apo, the apoenzyme with phosphate bound (6G4C, 1.87 Å resolution with an R_{free} of 0.184); *Pj*TA-as, the apoenzyme with succinate bound (6G4B, resolution 1.80 Å, R_{free} = 0.203), and *Pj*TA-plp, the PLP-bound enzyme (6G4D, 2.15 Å resolution, R_{free} = 0.261). For each point mutation, the $\Delta\Delta G^{fold}$ value was calculated using Rosetta[38] with the Row 3 protocol (options: -ddg::local_opt_only true−ddg::opt_radius 8.0−ddg::weight_file soft_rep_design -ddg::iterations 50-

https://dx.doi.org/10.1021/acscatal.9b05223
ACS Catal. 2020, 10, 2915−2928

ddg::min_cst false-ddg::mean true-ddg::min false-ddg::sc_min_only false-ddg::ramp_repulsive false). The same calculations were performed with FoldX[39] using its standard settings. All FoldX calculations were repeated five times to obtain better averaging (Table S4). For both the FoldX and the Rosetta protocol, the results over the three dimeric TA structures were averaged.

To eliminate mutations that are unlikely to be stabilizing, we used visual inspection of MD trajectories, which is a standard part of the FRESCO procedure and described in detail elsewhere.[37] For each mutant, a 3D structure was predicted by FoldX using the crystal structure of the wild-type *Pj*TA-plp as the template. The modeled structure of each mutant was the starting point for five independent YASARA MD simulations[40] of each 100 ps. The visual inspections, which were also recently described in detail, result in the dismissal of mutations causing solvent exposure of hydrophobic side chains, introduction of unsatisfied H-bond donors and acceptors, increased flexibility, and other structural problems. Scripts and detailed protocols for the FRESCO procedure are available via https://groups.google.com/forum/#!forum/fresco-stabilization-of-proteins. Using this procedure, a computationally designed library of 226 variants was obtained for experimental verification.

For the consensus approach, homologues of *Pj*TA were searched using Blast and the nonredundant protein database at the NCBI. In total 179 homologous protein sequences were retrieved and used for multiple sequence alignment (MSA), using ConSurf to calculate a consensus sequence.[41] For each position in the sequence, the most abundant amino acid was identified as the consensus amino acid. The *Pj*TA sequence differed at 91 positions from the consensus sequence. The structures of all the individual back-to-consensus point mutations were visually inspected as described above to discard mutations with structural defects. This way, a small library with 10 potentially stabilizing point mutations was selected.

Several computational analyses were done independently from the selection process of mutants for experimental characterization. We examined the use of more stringent energetic criteria for mutant selection, similar to the protocol published by Bednar et al. under the acronym FireProt.[26] It uses the same FoldX settings as FRESCO (see above) with the Row 16 protocol of Rosetta. The prediction accuracy of the computationally more expensive Row 16 protocol is comparable to that of the Row 3 protocol used for FRESCO (for a large benchmark set of mutations with known $\Delta\Delta G^{fold}$ values the correlation coefficient R was 0.68 for the Row 3 protocol and 0.69 for the Row 16 protocol).[38] The settings for this protocol were -ddg::weight_file soft_rep_design -ddg::iterations 20-ddg::local_opt_only false-ddg::min_cst true -ddg::mean false -ddg::min true-ddg::sc_min_only false-ddg::ramp_repulsive true. These settings differ from the Row 3 protocol (shown above); the Row 16 protocol uses energy minimization of the entire protein, while the Row 3 protocol performs energy minimization only on amino acid side chains that are within 8 Å of the mutated residue.

B-fitter rankings of potential target positions in *Pj*TA were generated according to the manual provided by the Reetz group (http://www.kofo.mpg.de/en/research/biocatalysis).[42,43] The *B* factors of all non-hydrogen atoms of each residue were averaged for each position using the three aforementioned X-ray structures. Positions with the highest average *B* factor obtained the highest ranks.

To evaluate the existence of strain in the wild-type *Pj*TA at position Ile154, YASARA-Structure molecular modeling software was used.[44] The highest resolution X-ray structure of wild-type *Pj*TA (6G4B) was taken. For both subunits, first the dihedral angle of interest (of Ile154 the following atoms: C, Cα, Cβ, and Cγ1) was measured as well as the total van der Waals (Lennard−Jones) energy and dihedral energy of the protein. Subsequently, this dihedral was set to the nearest ideal value (−60°), after which those energies were measured again. The difference between both energies before and after setting the dihedral was reported. The employed force-field was Amber14.[45] For the detection of strain effects, the advantage of the use of this force field is that it has simple separate terms for van der Waals (Lennard−Jones) and dihedral energies.

Genetic Engineering, Enzyme Expression, and Purification. The vector pET-20b (+)-His-*Pj*TA, containing an in-frame fusion of the *Pj*TA gene with the ATG start codon, was described in our previous work.[12] Mutations of *Pj*TA were created by QuikChange site-directed mutagenesis. Primers were designed by the QuikChange Primer Design Program of Agilent Technologies. The mutations were verified by DNA sequencing (Eurofins Genomics). For library screening, we used small-scale enzyme production. Confirmed mutated plasmids were transformed into *E. coli* BL21(DE3) for expression. Single colonies were picked and grown overnight in 96-deep-well plates. Next, the cultures were transferred to 24-deep-well plates containing Terrific Broth (TB) medium with 100 μg/mL ampicillin and growth was continued at 37 °C until the OD_{600} value reached 0.6. Then the cultures were cooled to 24 °C and IPTG was added to a concentration of 1 mM. After further growth at 24 °C for 16 h, the cells were harvested by centrifugation at 3000*g* for 30 min and the pellets were washed and suspended with lysozyme solution (1 mg/mL lysozyme, 0.5 mg/mL DNase, 10 mM $MgCl_2$, 20 mM Tris-HCl, 150 mM NaCl, 20 μM PLP, pH 7.5). The suspensions were kept at −80 °C for 45 min and thawed under tap water to disrupt the cells. The plates were centrifuged at 3000*g* for 45 min at 4 °C, and some of the supernatant was used to determine enzyme production by SDS-PAGE. The remainder of the supernatants was loaded on AcroWell 96-well filter plates (Pall, USA) containing TALON metal affinity chromatography resin (Clontech, USA). Elution was conducted with buffer containing 20 mM Tris-HCl, 150 mM NaCl, 500 mM imidazole, and 20 μM PLP, pH 7.5. The desalting step was done with a multiwell gravity column PD MultiTrap G-25 (GE, U.K.) to remove imidazole. Enzymes were stored in buffer (50 mM potassium phosphate, pH 8.0) at −20 °C until use.

Selected promising variants were expressed and purified on a larger scale. After inoculation and overnight growth of precultures, the cells were transferred to 500 mL of TB medium (100 μg/mL ampicillin) and cultures were shaken at 37 °C. When the OD_{600} value reached 0.6, the temperature was lowered to 24 °C, and induction was started by addition of 1 mM of IPTG. After 16 h of growth the cells were collected at 7000*g* for 30 min and the pellets were washed and suspended in buffer (20 mM Tris-HCl, 500 mM NaCl, 20 μM PLP, pH 7.5). After sonication (15 min, 5 s intervals), the lysate was centrifuged at 36000*g* for 45 min at 4 °C. The supernatant was loaded onto a 5 mL HisTrap column (GE Healthcare, Sweden) and the enzyme was isolated with an AKTA purifier

https://dx.doi.org/10.1021/acscatal.9b05223
ACS Catal. 2020, 10, 2915−2928

using a linear gradient of 0 to 500 mM imidazole in buffer. Fractions containing the enzyme as judged by SDS-PAGE were pooled and desalted in phosphate buffer (50 mM potassium phosphate, pH 8.0) with Econo-Pac 10DG columns (Bio-Rad, USA). The purity was checked by SDS-PAGE, and the protein was quantified with the Bradford assay. Purified enzymes were stored in aliquots at −80 °C in 50 mM potassium phosphate, pH 8.0.

Thermal Shift Assays. T_m^{app} values were determined by the fluorescence-based Thermofluor assay.[46] Specifically, 5 μL of 50-fold diluted SYPRO orange and 20 μL of 0.5 mg/mL enzyme solution were placed in an IQ 96-well PCR plate (Bio-Rad, USA) and mixed thoroughly in the wells. The plates were sealed with Microseal B adhesive sealer (Bio-Rad, USA) and heated from 20 to 99 °C in a MyiQ real-time PCR machine (Bio-Rad, USA) with a linear gradient of increasing temperature (1 °C/min). The temperature at the maximum rate of fluorescence change (dRFU/dT) was taken as T_m^{app}.[47]

Activity Assays and (*S*)-1-PEA Synthesis. TA activities were measured by following the formation of acetophenone from (*S*)-1-PEA at 37 °C in 96-well MTP format. The reaction mixtures contained the substrates (*S*)-1-PEA and pyruvate at varying concentrations, 0.05 mM PLP, and 0.02 mg/mL of purified enzyme in 50 mM potassium phosphate buffer, pH 8.0. The formation of acetophenone was detected at 245 nm (extinction coefficient 12 mM^{-1} cm^{-1}).[48]

The synthesis of (*S*)-1-PEA from acetophenone was conducted at a concentration of 1 M IPA as amino donor and 20 or 100 mM acetophenone in 50 mM potassium phosphate, pH 8.0, containing 20% DMSO, 0.5 mM PLP, and 1 mg/mL of enzyme. Reactions were done at the enzyme's temperature optimum. The formation of (*S*)-1-PEA was measured by HPLC. Samples from reaction mixtures with enzymes were quenched by adding half a volume of 10% perchloric acid to samples taken at different reaction times, and precipitates were removed by centrifugation. Next, 200 μL of the supernatant of each sample was transferred to an HPLC vial for analysis. The formation of (*S*)-1-PEA was analyzed using a Crownpack CR (+) column (Daicel, Japan) with 0.6 mL/min perchloric acid (pH 1.5) for elution and detection at 210 nm.[49] Under these conditions, (*S*)-1-PEA eluted at 21 min with clear separation from (*R*)-1-PEA (27 min).

Crystal Structures. *Pj*TA variants R4 and R6 were further purified by size exclusion chromatography using a Superdex200 10/300 column (GE Healthcare, Sweden), equilibrated with 20 mM HEPES, pH 7.5, 100 mM NaCl, and 20 μM PLP. The purified enzymes were concentrated to ∼10 mg/mL using a Vivaspin Turbo 4 10K filter unit (Sartorius). Hanging drop vapor diffusion experiments were set up in 24-well LINBRO plates (Molecular Dimensions Ltd.) by mixing 1 μL of the protein solution with 1 μL of the reservoir solution containing 0.7−1.0 M sodium succinate, pH 7.6, similarly as used previously for crystallizing the wild-type *Pj*TA.[12] Single *Pj*TA R4 crystals appeared after 2 days and grew to an average size of 0.3 × 0.3 × 0.2 mm^3. Their yellow color indicated that PLP was bound. Large single yellow crystals were also obtained for R6 (average size 0.5 × 0.4 × 0.2 mm^3) but required a lower protein concentration of 5 mg/mL. Prior to data collection, crystals were soaked in a cryoprotectant solution containing 1.2 M succinate, pH 7.6, 0.1 mM PLP, and 30% glycerol. X-ray diffraction data for R4 were collected in house using Cu Kα radiation from a Bruker Microstar rotating-anode generator equipped with Helios MX mirrors. For R6, X-ray diffraction data were collected at beamline ID30A-3 at the European Synchrotron Radiation Facility (Grenoble, France). The diffraction data for R4 and R6 were indexed and integrated using iMOSFLM[50] and XDS,[51] respectively, and then scaled and merged using Aimless[52] from the CCP4 software suite.[53] The crystals of R4 and R6 belonged to the same space group as for wild-type *Pj*TA, with nearly identical unit cell dimensions, allowing the wild-type crystal structure (PDB entry 6G4B) to be directly used for initial refinement and electron-density map calculations. Subsequently, the structures were adjusted by model building to replace the side chains of the mutated residues. A few cycles of refinement using RefMac5,[54] alternated with model building and water placement using Coot,[55] were sufficient to complete the structures. A summary of data collection and model refinement statistics is provided in Table S1. Figures were produced with PyMol.[56]

RESULTS AND DISCUSSION

Computational Library Design. In view of the instability of dimeric class III TAs[9] and the importance of enzyme robustness for biocatalytic applications, we investigated the possibility to enhance the stability of the homodimeric *Pj*TA by protein engineering. For this we chose the FRESCO workflow, which was used earlier by us and others to increase the thermostability of dimeric limonene epoxide hydrolase (ΔT_m^{app} = 35 °C),[30] monomeric haloalkane dehalogenase (ΔT_m^{app} = 23 °C),[31] monomeric peptide amidase (ΔT_m^{app} = 23 °C),[32] monomeric xylanase (ΔT_m^{app} = 14 °C),[33] monomeric HMF oxidase (ΔT_m^{app} = 11 °C),[34] monomeric cyclohexanone monooxygenase (ΔT_m^{app} = 13 °C),[35] and a tetrameric halohydrin dehalogenase (ΔT_m^{app} = 28 °C).[36] First, all possible point mutations were subjected to folding energy calculations. FoldX and Rosetta predicted 385 and 883 potentially stabilizing point mutations ($\Delta\Delta G^{fold}$ < −2.5 kJ/(mol subunit)), respectively, with some overlap. To further computationally enrich this virtual library, all 1028 different mutants substituted at 222 different positions were subjected to MD simulations and brief on-screen inspection. Discarding mutants with structural defects or increased local flexibility yielded a reduced virtual library of 226 point mutations at 114 different positions which qualified for experimental testing. This set included 20 buried mutations, 172 surface mutations, 32 interface mutations, and 2 mutations located at both the surface and the interface (Table S2).

After multiwell plate format QuikChange mutagenesis and transformation to *E. coli* BL21(DE3), 204 of the 226 sequenced mutants gave expression of enzyme in soluble form as shown by SDS-PAGE. For the 22 other sequence-verified variants, the gels showed that no target protein was produced and also no signal was found in Thermofluor assays after His-tag purification in multiwell format. We initially tested a set of surface-located mutations, hoping to find useful variants, but the stabilizing effect was small. When all 204 expressed mutants were tested, 29 significantly stabilizing point mutations were discovered in Thermofluor assays ($\Delta T_m^{app} \geq$ +1 °C, from triplicate assays) and these were distributed over 16 different positions (Table 1). Of the confirmed stabilizing mutations, 17 were located at the subunit interface and 10 mutations were located at the surface; 2 additional mutations (E74I and N78K) were located at the border of the surface and the interface. These numbers show that of the 172 predicted surface mutations that were not at the interface, only 6% were stabilizing, whereas of the selected 34 interface mutations, 56%

https://dx.doi.org/10.1021/acscatal.9b05223
ACS Catal. 2020, 10, 2915−2928

Table 1. Stabilizing Point Mutations Discovered in *Pj*TA

mutation	location	origin	$\Delta\Delta G^{fold}$ (kJ/mol)[a]	ΔT_m^{app} (°C)[b]
P9A	surface	Rosetta	−4.3	2
P9K	surface	Rosetta	−7.4	1.5
E38K	surface	Rosetta	−9.9	1.5
E38Q	surface	Rosetta	−5.5	2
A60V	interface	consensus		4
E74I	surface, interface	FoldX, Rosetta	−7.8, −11.2	5.5
N78K	surface, interface	Rosetta	−4.1	1
F86W	interface	Rosetta	−12.9	4
S87D	interface	FoldX	−3.0	7
S87H	interface	Rosetta	−15.1	1
S87N	interface	FoldX, Rosetta	−4.1, −9.9	1.5
S87Q	interface	FolX, Rosetta	−3.8, −4.8	1
K89A	interface	Rosetta	−4.4	2
K89F	interface	FoldX, Rosetta	−6.2, −19.0	6
K89L	interface	FoldX	−7.4	4.5
K89M	interface	FoldX	−3.7	3.5
K89W	interface	Rosetta	−15.9	3.5
K89Y	interface	Rosetta	−16.6	4
S94A	interface	Rosetta	−9.4	8
S110Q	surface	FoldX, Rosetta	−3.8, −4.7	1
M128F	interface	FoldX, Rosetta	−5.0, −15.5	4.5
P139 K	surface	Rosetta	−3.2	1
N149G	surface	FoldX	−3.0	2.5
I154D	interface	Rosetta	−3.2	4
I154N	interface	Rosetta	−7.0	3.5
I154V	interface	Rosetta, consensus	−10.3	9
L227V	surface	consensus		1
L319F	interface	FoldX, Rosetta	−6.9, −4.9	4
A393R	surface	FoldX	−3.9	1.5
M419I	surface	Rosetta	−6.2	1
M419L	surface	Rosetta	−4.2	1.5

[a]The $\Delta\Delta G^{fold}$ energies are calculated by FoldX and/or the Rosetta Row 3 protocol; values are per monomer. [b]The ΔT_m^{app} value of wild-type *Pj*TA (WT) is 62 °C.

improved thermostability. Moreover, the degree of stabilization by surface mutations was modest (+1 °C ≤ ΔT_m^{app} < +3 °C), except for mutation E74I (+5.5 °C), which is partially at the interface. The interface mutations caused a much larger increase in stability, with 74% of the interface-located stabilizing mutations giving $\Delta T_m^{app} \geq$ +3 °C (Figure 1). Thus, interface point mutations stabilized *Pj*TA much better than surface mutations, which confirms the hypothesis that subunit interactions are crucial to TA stability.

These results indicate that mutations stabilizing the interface can be rapidly discovered by computational design. The high abundance (56%) of experimentally confirmed stabilizing mutations in a small set of only 34 interface mutants suggests that, for proteins where stability is due to subunit dissociation, it is possible to strongly reduce the library size for experimental testing in comparison to usual random directed evolution protocols. The high success rate also compares favorably to that of FRESCO mutations which are selected without focusing on suspected sensitive regions (success percentages

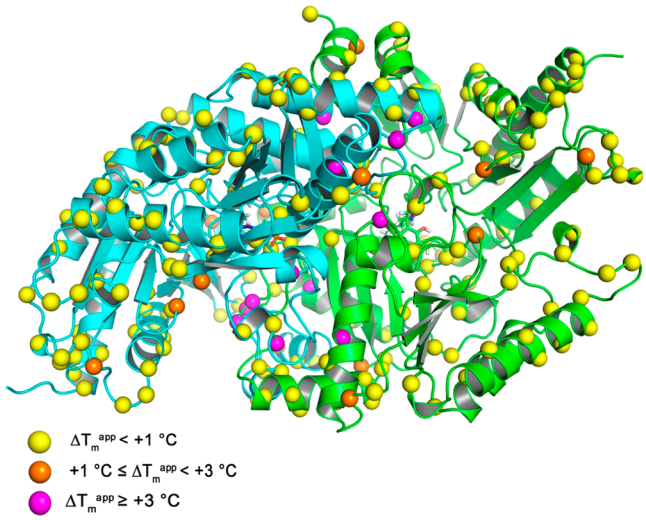

Figure 1. Spatial distribution of *Pj*TA point mutations influencing thermostability. The colored spheres indicate the highest positive ΔT_m^{app} observed at a position. Yellow spheres indicate that no stabilization was observed.

of ca. 10−20% for 8 different proteins including the current target (Table S3)). This suggests that focusing on sensitive regions in computational thermostability engineering can strongly reduce laboratory screening.

For *Pj*TA it transpires that the interface is far more relevant for stabilization than other areas and the most stabilizing mutation G98M (+4 °C) of *ω*-TA from *Variovorax paradoxus* was also at the interface.[57] However, this is not a general phenomenon for multimeric enzymes. For example, for a tetrameric halohydrin dehalogenase two critical regions were observed.[36] One of these critical regions was indeed at a subunit interface, but the other equally important region was at the surface. In a dimeric limonene epoxide hydrolase that was also targeted by FRESCO, several of the most stabilizing mutations were also not at the interface.[30] Focusing exclusively on the subunit interfaces in those enzymes would have missed many strongly stabilizing mutations.

With other methods, it also remains challenging to predict the region that is critical for thermostability. A well-known approach is the *B*-fitter method, which predicts critical residues on the basis of high *B* factors.[42,43] However, in the case of *Pj*TA, only 1 out of the 16 positions where stabilizing mutations were observed showed a significantly high *B* factor in the wild-type crystal structures (Table S2). Thus, most of these mutations would escape discovery by the *B*-fitter approach for stability engineering. After averaging and ranking of *B* factors in the wild-type crystal structures, only E38K/Q (T_m^{app} = 1.5/2.0 °C) had a high ranking according to its *B* factor (rank 25). All other stabilizing residues with the highest *B* factor appeared after the 30th rank, which is outside the proposed threshold.[43] Nevertheless, focusing on high *B* factor regions did yield mutations that improve the stability of *Chromobacterium violaceum* TA (*Cv*TA).[58] For the one enzyme that has been improved both by FRESCO and by the *B*-fitter approach (halohydrin dehalogenase), the two approaches found different stabilizing mutations,[36,59] indicating that they may be complementary.

Unlike in earlier work with FRESCO, we averaged the results of the FoldX and Rosetta calculations obtained with three different X-ray structures instead of taking results from a

https://dx.doi.org/10.1021/acscatal.9b05223
ACS Catal. 2020, 10, 2915−2928

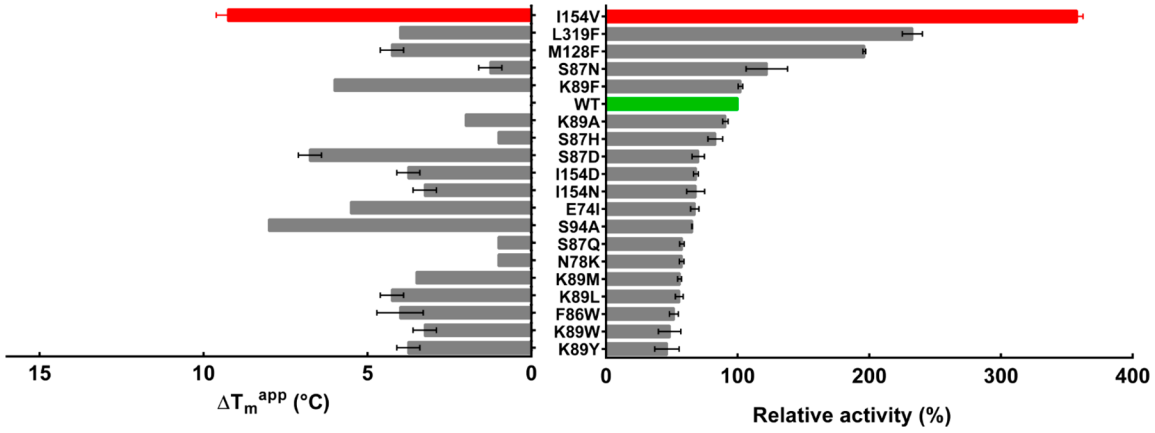

Figure 2. ΔT_m^{app} values and catalytic activities of *Pj*TA variants containing interface-stabilizing mutations. Activities were determined by measuring acetophenone formation from (*S*)-1-PEA with pyruvate as the amino acceptor (see Materials and Methods). WT had an activity of 13 U/mg (1 U equals 1 μmol/min). WT is shown as a green bar. The I154V mutants served as a template for adding mutations.

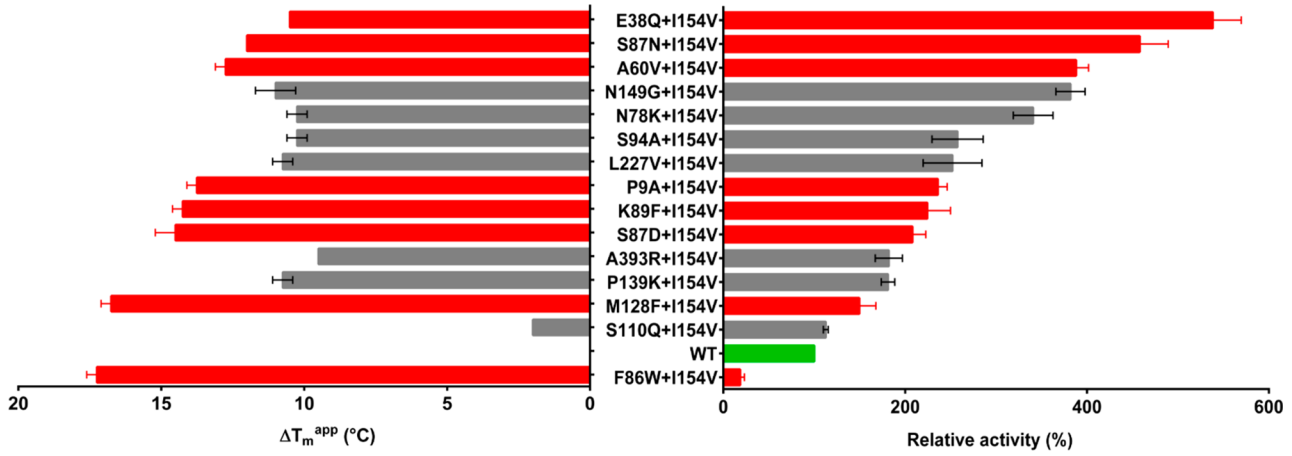

Figure 3. Catalytic activities and ΔT_m^{app} values of *Pj*TA double mutants. Activities were determined by measuring acetophenone formation from (*S*)-1-PEA with pyruvate as the amino acceptor. WT is shown as a green bar. Double mutants shown in red were selected as templates for further combination mutants.

single structure. A retrospective analysis showed that 3 out of the 31 stabilizing mutations could have been missed if only a single input structure were used: I154D with 6G4B and P9A and P139K with 6G4C. These substitutions just fail the chosen threshold of −2.5 kJ/(mol subunit) for experimental characterization (Table S4). Template selection and averaging can influence calculated $\Delta\Delta G^{fold}$ values and mutant selection, although the effect was small in this case.

Another approach to reduce the number of computationally designed mutations that need to be screened experimentally is the use of stricter criteria for predicted $\Delta\Delta G^{fold}$ values, as in the Fireprot protocol.[26] Our standard protocol uses $\Delta\Delta G^{fold} \leq -2.5$ kJ mol^{-1} per subunit for both FoldX and Rosetta. When only mutations were accepted with $\Delta\Delta G^{fold} \leq -4.184$ kJ mol^{-1} for FoldX and $\Delta\Delta G^{fold} \leq -8.368$ kJ mol^{-1} for Rosetta (FireProt criteria), only 28 instead of 226 mutations would qualify for experimental testing. Of those 28, 5 were indeed stabilizing (Table S2). The stricter energy criteria only slightly improved the fraction of successful mutations (from 14 to 17%), and the smaller set of 28 still included mutations that decrease thermostability. It should be noted that FoldX and Rosetta predict $\Delta\Delta G^{fold}$ at ambient temperature and not ΔT_m^{app}, which is far more difficult to model and is not strongly correlated to $\Delta\Delta G^{fold}$.

We also explored the use of consensus mutations to stabilize *Pj*TA. First, we used Blast searches to find homologues of *Pj*TA in the nonredundant protein database of the NCBI, and 179 different sequences were chosen. A consensus sequence, obtained by ConSurf,[41] differed from *Pj*TA at 91 positions. After point mutants with structural defects were discarded by visual inspection, a small library containing 10 potentially stabilized mutants was constructed and their stabilities were measured in the laboratory (Table S5). This yielded three confirmed stabilizing mutations (all with $\Delta T_m^{app} \geq +1$ °C; see Table 1), one of which was at the surface and two were at the interface. The interface mutation I154V is one of only two mutations shared between the FRESCO library and the consensus set, and with +9 °C it gave the largest ΔT_m^{app} value. Other stabilizing mutations are not shared, and about half of the mutations found by FRESCO are neither at positions that are strongly conserved among a set of 226 homologous TAs nor at positions where *Pj*TA deviates from strongly conserved residues in the consensus sequence, as indicated by ConSurf calculations (Figure S5). The results of comparing different strategies for enzyme stabilization will be strongly dependent on the way strategies are implemented and on the particular system under investigation. In the case of TAs we expect that the structure-based design of small libraries focusing on

https://dx.doi.org/10.1021/acscatal.9b05223
ACS Catal. 2020, 10, 2915−2928

mutations that stabilize the interface will be particularly effective.

Since most of the effective mutations are at the subunit interface and are close to the active site, there was a risk that they reduce activity or show antagonistic effects. When the effect of the individual stabilizing interface mutations on catalytic activity at 37 °C was examined, it appeared that most of them indeed gave somewhat lower activity in comparison to wild-type *Pj*TA (Figure 2). Gratifyingly, we also found interface mutations that strongly enhanced catalytic activity: i.e., K89F, S87N, M128F, L319F and I154V (Figure 2). I154V was especially effective, as it increased the activity by a factor of 3.5 and had a large positive effect on T_m^{app}. Stabilizing the subunit interface not only increased stability but could also improve activity.

Combining Stabilizing Mutations. In order to engineer a highly stable *Pj*TA, we rationally combined confirmed stabilizing mutations. Some interface mutations that enhanced stability but lowered activity were included, since it was considered that the activity could be recovered when mutations were combined. In the case of different stabilizing mutations at the same position, the mutation giving the most favorable effect on ΔT_m^{app} was selected. For example, mutation I154V, which gave +9 °C and 3.5-fold greater activity, was prioritized over I154N and I154D (Figure 2). The I154V mutation was included in all combination mutants. For position Ser87, variant S87D gave the best ΔT_m^{app} value (+7 °C) and S87N was the best for activity (1.2-fold increase); therefore, both were examined in combinations. Finally, nine interface stabilizing mutations, eight surface mutations, and two mutations that were partially at the interface were selected for combination.

On examination of *Pj*TA variants carrying different pairs of stabilizing mutations, it appeared that most mutations combined well with I154V, yielding several double mutants with ΔT_m^{app} value of +9 to +17 °C, with the exception of I154V + S110Q, which only displayed a 2 °C increase (Figure 3). In addition, activities improved by up to 5.4-fold over wild-type *Pj*TA. The only less active double mutant was I154V +F 86W (Figure 3). After it was shown that this combination strategy is feasible, 8 double mutants with decent activity and improved stability (I154V + E38Q, I154V + S87N, I154V + A60V, I154V + P9A, I154V + K89F, I154V + S87D, I154V + M128F and I154V + F86W) were selected as templates for introducing further mutations, resulting in triple mutants, 4-fold mutants, 5-fold mutants, and 6-fold mutants (Figures S1–S4). This yielded 27 different mutants with improved activity and stability.

From the set of combination mutants, six variants each with four to six mutations were selected for temperature–activity profiling, since it was considered possible that activity in some variants would be lower at the standard assay temperature of 37 °C but would improve at higher temperatures. For all six variants, the optimum temperature was increased, reaching values of 60–70 °C for some mutants, about 20–30 °C higher than the wild-type *Pj*TA optimum temperature (37 °C) (Figure 4). The activities at the new optimal temperatures of the robust mutants R4 (P9A + E38Q + S87D + I154V), R5 (P9A + E38Q + A60V + S87D + I154V) and R6 (P9A + E38Q + A60V + S87N + M128F + I154V) were up to 5-fold higher than the wild-type activity at 37 °C (Table 2). There was a 6.8-fold difference in activity at 37 °C between mutants R4 and R6, while their activities were almost the same at their

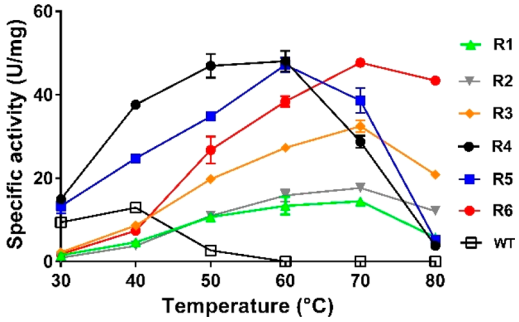

Figure 4. Temperature–activity profile of WT and stabilized variants of *Pj*TA. Activities were determined by measuring acetophenone formation from (*S*)-1-PEA with pyruvate as the amino acceptor.

respective optimum temperatures, pointing to quite different temperature dependences. Furthermore, the individual mutations of these two variants clearly showed additive effects on ΔT_m^{app} when they were combined. Therefore, these two robust *Pj*TA variants R4 and R6 were selected for further study (Table 2).

The T_m^{app} values of R4 and R6 (80 and 85 °C measured by thermal shift assays) are in the range of values (T_m^{app} > 80 °C) observed for enzymes from thermophilic organisms.[60] The impressive thermostability of the combination mutants and prominence of stabilizing interface mutations suggest that subunit dissociation is an important step in the irreversible inactivation pathway.[29] It has been proposed by Börner et al.[9] for three different TAs that dissociation from the enzyme of the aminated cofactor PMP formed in the first half reaction (Scheme 1) is a key step in activity loss, and strengthening of cofactor binding indeed enhanced stability.[8] In *Pj*TA, loss of the PLP or PMP cofactor will require dissociation of the dimer or partial protein unfolding, since the cofactor is buried between the two monomers and the phosphate group of each cofactor is bound by both subunits (Figure S6). Enhanced cofactor binding and increasing dimer stability are compatible mechanisms.

Stabilized *Pj*TAs Have Higher Activity, Thermostability, and Cosolvent Resistance. The catalytic properties of R4 and R6 were determined by initial rate assays in which (*S*)-1-PEA was used as the amino donor and pyruvate as the amino acceptor (Table 3). With these substrates, both stabilized variants showed a 4–5-fold higher k_{cat} value than wild-type *Pj*TA at their optimum temperatures, while the K_M values for (*S*)-1-PEA and pyruvate were both slightly increased. The k_{cat}/K_M values at their optimum temperatures were improved in comparison to wild-type *Pj*TA, for both the amino donor and acceptor. With a higher k_{cat} and lower K_M, variant R6 was slightly better for (*S*)-1-PEA conversion than R4.

To further examine the robustness of the selected mutants, the stabilities at high temperature were measured. The enzymes were incubated at different temperatures (30–80 °C) for 2 h. After they were cooled for 5 min at 4 °C, samples were withdrawn for activity assays at their optimum temperatures. From 30 to 40 °C, no difference in stability was found between wild-type *Pj*TA and mutants (Figure 5). Interestingly, during incubation at 30 °C for 2 h, the activities of both mutants increased, which may be due to enzyme refolding. Above 40 °C both the R4 and R6 variants were more stable than wild-type *Pj*TA, and the activities of the mutants only dropped slightly until 70 °C. For the wild-type *Pj*TA, no

https://dx.doi.org/10.1021/acscatal.9b05223
ACS Catal. 2020, 10, 2915–2928

Table 2. Properties of Selected Stabilized *Pj*TA Variants

variant	mutations	optimum temp (°C)	specific activity (U/mg)		T_m^{app} (°C)	PDB
			37 °C	temp opt		
WT		37	13 ± 0.1	13 ± 0.1	62	6G4B-F
R1	P9A + E38Q + S87D + M128F + I154V	70	2.7 ± 0.1	14.5 ± 0.2	86	
R2	P9A + E38Q + S87N + M128F + I154V	70	1.8	17.7 ± 0.8	86	
R3	P9A + E38Q + A60V + S87D + M128F + I154V	70	6.7 ± 0.1	32.5 ± 1	86	
R4	P9A + E38Q + S87D + I154V	60	37.7	48 ± 1.7	80	6TB0
R5	P9A + E38Q + A60V + S87D + I154V	60	24.8 ± 0.1	47.2 ± 1.2	81	
R6	P9A + E38Q + A60V + S87N + M128F + I154V	70	5.5 ± 0.1	47.7 ± 0.2	85	6TB1

Table 3. Kinetic Properties of WT and Two Stabilized Variants

enzyme	T_m^{app} (°C)	k_{cat} (s^{-1})	(*S*)-1-PEA		pyruvate	
			K_M (mM)[a]	k_{cat}/K_M (mM^{-1} s^{-1})	K_M (mM)	k_{cat}/K_M (mM^{-1} s^{-1})
WT	62	12.7 ± 0.1	9.6 ± 1.2	1.4 ± 0.1	4.4 ± 0.5	3.0 ± 0.3
R4	80	56.7 ± 1.0	13.1 ± 1.6	4.4 ± 0.6	10.6 ± 1.6	5.5 ± 0.9
R6	85	58.2 ± 0.8	11.5 ± 1.7	5.2 ± 0.8	13.5 ± 1.8	4.4 ± 0.6

[a]Initial rates were determined by measuring acetophenone formation with varying concentrations (0−32 mM) of (*S*)-1-PEA as the amino donor and 50 mM pyruvate as the amino acceptor or with 50 mM (*S*)-1-PEA as the mino donor and varying concentrations (0−32 mM) of pyruvate as the amino acceptor.

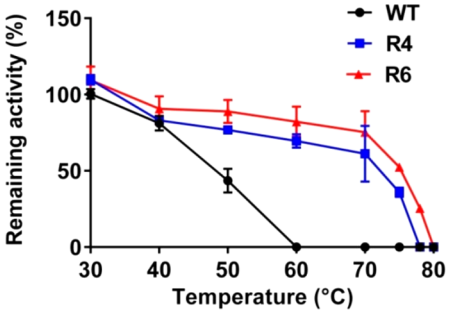

Figure 5. Comparison of thermal stabilities of WT and thermostable variants R4 and R6. Enzymes were incubated at the indicated temperatures for 2 h, and the assays were carried out after dilution of the enzymes in the buffer (50 mM potassium phosphate, pH 8.0). Activities were determined by measuring acetophenone formation from (*S*)-1-PEA with pyruvate as the amino acceptor. The remaining activity was measured at the optimum temperature of each individual variant.

activity was found with enzyme incubated at 60 °C or higher. Mutant R6 was always slightly more stable than R4. The increased stability observed in these thermal shock assays for R4 and R6 correlated with the enhanced T_m^{app} values obtained from thermal shift assays (Table 3).

Another important aspect of enzyme robustness is stability in the presence of organic solvents. Two often-used organic solvents were examined, dimethyl sulfoxide (DMSO) and methanol. The variants R4 and R6 were incubated with 20% cosolvent at 30 °C. After 2 h, samples were withdrawn to assay for (*S*)-1-PEA deamination at the respective optimum temperatures in buffer without additional solvent. We found almost no activity loss with the stable variants (Figure 6A). In contrast, the wild-type *Pj*TA activity dropped by approximately 48% and 20% after 2 h incubation with 20% DMSO and 20% methanol, respectively.

In view of the robustness of R4 and R6 in DMSO and methanol, deamination reactions were also conducted in the presence of 20% cosolvent. Both R4 and R6 were much more active than wild-type *Pj*TA, the highest activity being observed for R6 (Figure 6B). We also found that methanol is a more suitable cosolvent for deamination reactions in comparison to DMSO, for both variants as well as for wild-type *Pj*TA.

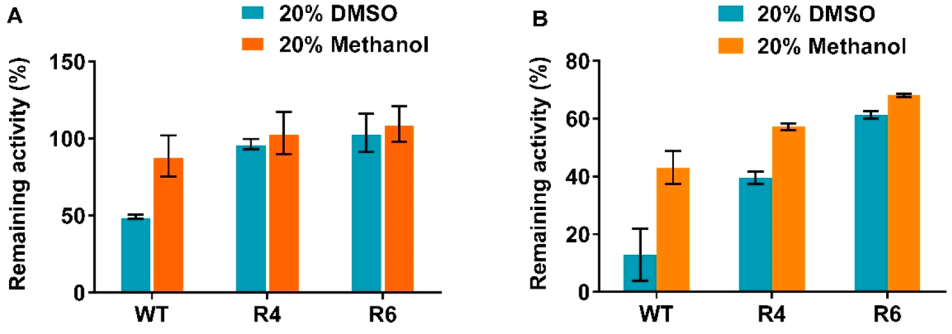

Figure 6. Enhanced stability of *Pj*TA variants in cosolvents. The remaining activity was measured at the optimum temperature of each individual variant. (A) Residual (*S*)-1-PEA deamination activity after incubation with DMSO or methanol as cosolvent (20% v/v) of wild-type *Pj*TA and variants R4 and R6. The enzymes were preincubated at 30 °C in cosolvents for 2 h prior to assays. The assays were carried out after dilution of the enzymes in cosolvent-free buffer. (B) Effect of cosolvents on (*S*)-1-PEA deamination activities. Activities were measured in the presence of 20% cosolvent.

https://dx.doi.org/10.1021/acscatal.9b05223
ACS Catal. 2020, 10, 2915−2928

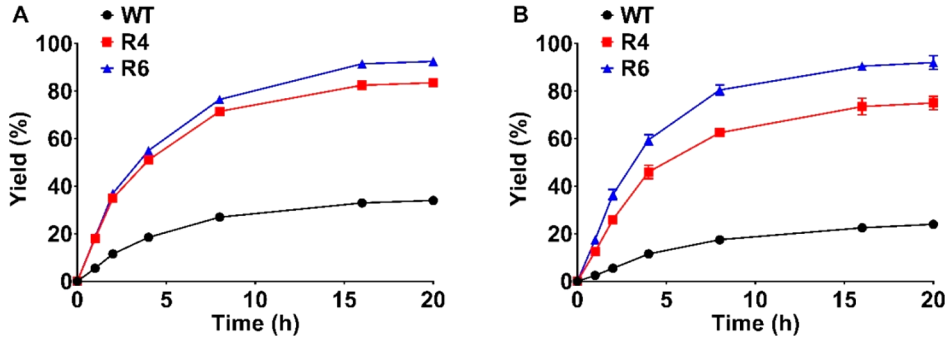

Figure 7. Conversion of acetophenone to (*S*)-1-PEA by WT and the two robust variants R4 and R6. In all cases, the concentration of the IPA amino donor was 1 M, the PLP concentration was 0.5 mM, and enzymes were added at 1 mg/mL. The reactions were measured at the optimum temperature of each individual variant. (A) Initial concentration of acetophenone 20 mM. (B) Initial concentration of acetophenone 100 mM with 20% DMSO.

The stability increases make *Pj*TA a highly robust enzyme, also in comparison with the well-studied dimeric ω-TAs from *C. violaceum* (*Cv*TA) and *Vibrio fluvialis* (*Vf*TA). Whereas wild-type *Pj*TA seems more unstable than some of its homologues, the R4 and R6 mutants of *Pj*TA have surpassed other ω-TAs in stability. Engineered homotetrameric *Pseudomonas* sp. ω-TA, investigated by Börner et al.,[9] still had lost activity after a 2 h incubation at 62 °C, while R4 and R6 were still active (Figure 5). Similarly, no activity loss was found for R4 and R6 upon incubation for 2 h in 20% DMSO or 20% methanol (Figure 6A), whereas thermostable ω-TA from *Thermomicrobium roseum* (ω-TATR) retained only about 50% or 75% activity, respectively.[60]

Increased IPA Tolerance in Amine Synthesis. In view of the stability of R4 and R6, we also examined the tolerance to a high concentration of IPA, a preferred cheap amino donor for ω-TA-catalyzed reactions.[61,62] Tolerance is important because IPA needs to be used in excess over the acceptor for the efficient production of amines, especially in case of unfavorable reaction equilibria. To determine the tolerance of the R4 and R6 variants, reactions were done with an IPA concentration of 1 M, which is 50-fold higher than the concentration of the amino acceptor acetophenone. After 20 h of incubation at each optimum temperature, the conversions of acetophenone to (*S*)-1-PEA were 84% and 93% for R4 and R6, respectively, in comparison to 35% conversion with the wild-type *Pj*TA (Figure 7A). The initial rates were higher for the mutants, in the case of both R4 (60 μM/min) and R6 (63 μM/min), in comparison to wild-type *Pj*TA (20 μM/min). Thus, the two robust mutants accepted IPA better as an amino donor and gave a 2.5-fold increase in yield. The enantioselectivities were not changed (ee >99%, for both wild-type *Pj*TA and the two variants). Mutants of a TA from *Ruegeria* sp. TM1040 (PDB: 3FCR) that show very good conversion of acetophenone and 2-bromoacetophenone were reported by Dawood et al.[63] In that case, three to four mutations were introduced in the active site to enhance activity in reactions with IPA as the amino donor. The improvement may be related to better acceptance of the ketone substrate, reducing the lifetime of the vulnerable PMP-enzyme intermediate in the catalytic cycle. Reduced dissociation of the PMP-enzyme was also proposed for the transaminase mutants engineered by Börner et al.[8,9] Thus, three ways of improving TAs for better ketone or aldehyde to amine conversion with IPA as amine donor emerge: reducing dissociation of the native enzyme assembly into subunits, enhancing binding of the PLP cofactor, and improving the binding and reaction of the ketone or aldehyde amine acceptor.

To further verify the robustness of R4 and R6, the amination reaction was also conducted with cosolvents. In the reaction, the amino donor IPA was kept at 1 M and 100 mM acetophenone substrate was dissolved with 20% DMSO. After a 20 h reaction time, the conversions of acetophenone to (*S*)-1-PEA were 75% and 92% for R4 and R6, respectively, in comparison to 24% conversion with the wild-type *Pj*TA (Figure 7B). Thus, the performance of two robust variants was indeed better with cosolvents. Especially for R6, the fraction of conversion remained the same even though the substrate concentration was 5-fold higher.

Crystal Structures of Robust *Pj*TA Variants. To understand the structural basis of the enhanced thermostability and to assess the reliability of the computational prediction methods, structures were determined for the R4 and R6 variants. The crystal structures were refined to 1.95 Å resolution with an *R* factor of 0.139 (R_{free} = 0.172) for R4 and to 1.85 Å resolution with an *R* factor of 0.144 (R_{free} = 0.173) for R6. Both crystal structures contain the PLP cofactor as an internal aldimine, covalently linked to Lys287. They have good stereochemistry, and no significant differences were observed in overall backbone conformation between the wild-type and mutant *Pj*TA structures. All mutated residues displayed well-defined electron density, allowing unambiguous assignment of their side-chain conformations and a clear analysis of interactions with neighboring residues.

Mutation P9A, present in both variants, is located at the N-terminus of a short α-helix (Figure 8A,B). The experimental and predicted structures for this mutation are in excellent agreement, revealing no significant differences in local protein structure. The mutation occurs at the second residue composing the α-helix (α1), located at the N-terminus of the protein. The hydrophobic side chain of Pro9 is fully exposed to solvent, and its substitution with a small methyl group is expected to improve protein surface solvation. Furthermore, unlike the amide group of Pro9, the backbone amide group of Ala9 is able to form a hydrogen bond with water, as is evident from the crystal structures of R4 and R6. Thus, the improvement in stability of the P9A mutation is explained by a combination of reduced exposed hydrophobic surface and improved protein−water interactions.

Mutation E38Q also occurs at the protein surface. In the crystal structures of the mutants, residue Gln38 adopts a side chain rotamer different from that predicted (Figure 8C,D), but

https://dx.doi.org/10.1021/acscatal.9b05223
ACS Catal. 2020, 10, 2915−2928

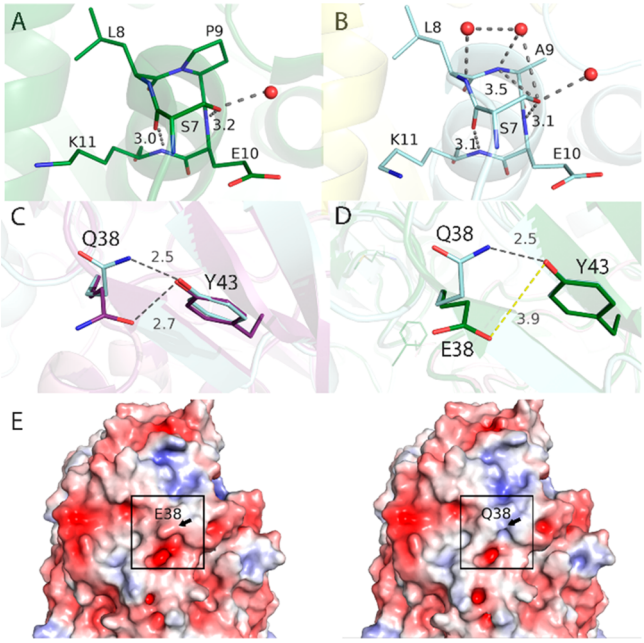

Figure 8. Structural analysis of the mutations P9A and E38Q. (A) Wild-type *Pj*TA crystal structure showing Pro9 and surrounding residues (sticks) after the α-helical N-cap, stabilized by hydrogen bonds within the helix (gray dashed lines). A water forming a hydrogen bond with the carbonyl oxygen of Pro9 is shown as a red sphere. Distances are in Å. (B) A similar representation of the R4 crystal structure showing Ala9 as sticks and interacting waters as red spheres. Waters form a hydrogen-bonding network with the backbone and the side chains of residues at the N-terminus of the helix, which is not observed in the wild-type structure. (C) Overlay of the R4 crystal structure (cyan) with the predicted structure (purple), showing the hydrogen-bond interactions of Gln38 with Tyr43 (dashed gray lines). (D) Similar overlay of the R4 crystal structure (cyan) with the wild-type crystal structure (green). Distances are in Å. (E) Comparison of the electrostatic surface around residue 38 (arrow) in wild-type *Pj*TA (left) and in the R4 variant (right). The E38Q mutation results in a more even distribution of positive (blue) and negative (red) surface charges, highlighted in the boxed area.

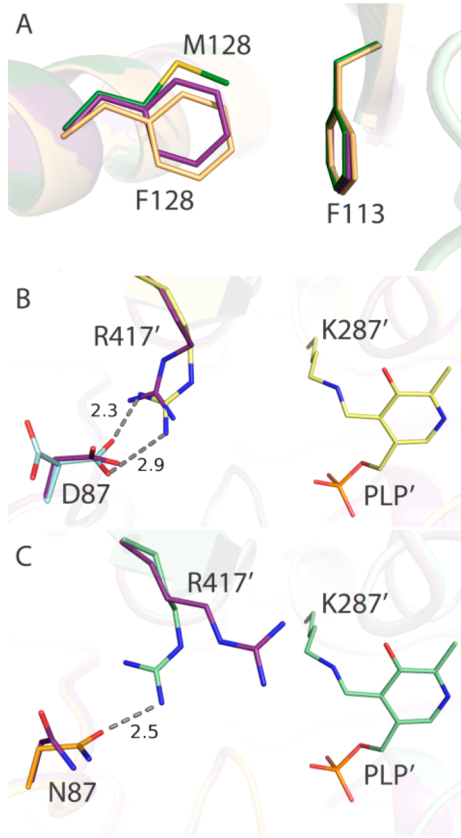

Figure 9. Structural analysis of mutations M128F, S87D, and S87N. (A) Overlay of the R6 crystal structure (orange) with the predicted structure (purple) and wild-type crystal structure (green), showing mutation M128F and neighboring residue Phe113 (sticks). The phenyl rings of Phe128 and Phe113 are ideally positioned for a T-shaped $\pi-\pi$ interaction. (B) Overlay of R4 crystal structure (chain A in cyan, chain B in yellow) with the predicted structure (purple), showing how Asp87 forms a salt bridge with the arginine switch Arg417′ across the dimer interface. (C) Overlay of the R6 crystal structure (chain A in orange, chain B in pale green) with the predicted structure (purple), showing how Arg417′ in R6 adopts a conformation similar to that in R4 by forming a hydrogen bond with Asn87. The interaction is absent in the predicted structure, where Arg417′ has a different conformation facing the active site. Distances are given in Å.

in both conformations the side chain forms a hydrogen bond with the hydroxyl group of Tyr43. In the wild-type crystal structure, residue Glu38 due to a salt bridge with Arg36 does not form hydrogen bonds with neighboring residues, so that the enhancement in stability can partially be explained by improved hydrogen-bonding interactions on the surface. In addition, the removal of the negative charge by the E38Q mutation reduces unfavorable electrostatic interactions on the protein surface (Figure 8E), which may also contribute to better protein stability.[17]

Mutation A60V was obtained by the consensus approach. In comparison to the alanine residue in the wild-type structure, Val60 in the R6 crystal structure forms additional apolar van der Waals contacts with the side chains of Phe64 and Phe82′; the latter are not present in the wild type. The stabilizing effect of the mutation can thus be attributed to improved hydrophobic packing interactions of side chains at or near the dimer interface.

For mutation M128F, occurring only in R6, the experimental and predicted structures are in excellent agreement. The improvement in stability is clearly related to the new T-shaped $\pi-\pi$ interaction between Phe128 and Phe113 (Figure 9A).

The contribution to stability of the Ser87 mutants (S87D in R4, S87N in R6) is related to improved contacts at the dimer interface. In the R4 crystal structure, the side chain of Asp87 shows alternate conformations. In one of the conformations the carboxylate forms a salt bridge with Arg417′, similar to the salt bridge in the predicted structure of the S87D mutant (Figure 9B). The formation of a salt bridge at the dimer interface is consistent with the significant increase in T_m^{app} for this mutation. Also, Asn87 in the R6 crystal structure interacts with Arg417′, but via a hydrogen bond (Figure 9C), which is normally a weaker interaction, consistent with the smaller increase in T_m^{app} for mutation S87N. In the predicted structure containing the S87N mutation, the side chain of Arg417′ points away from Asn87 toward the active site. In this configuration the Arg417′ guanidinium group is exposed to solvent. This indicates that the small improvement in stability for S87N could also be due to improved solvation of the Arg417′ side chain. Differences in interactions of Arg417′ may also explain the opposite effects on activity observed for the

https://dx.doi.org/10.1021/acscatal.9b05223
ACS Catal. 2020, 10, 2915−2928

two mutations. The arginine is strictly conserved in ω-TAs and plays an important role in catalysis by a conformational change called an arginine switch, which enables dual substrate recognition.[64] During conversion of (*S*)-1-PEA in *Pj*TA, Arg417′ needs to move out of the active site tunnel to allow binding of the substrate's phenyl group. However, during the second half-reaction it moves in to interact with the carboxylate group of pyruvate, facilitating its conversion to L-Ala. Thus, the lower activity caused by the S87D mutation is consistent with the formation of a salt bridge with Arg417′, as it deprives the active site of a residue involved in the catalysis, while the increase in activity for the S87N mutation may be related to an increase in flexibility of the Arg417′ side chain.

Finally, for mutation I154V the crystal structures reveal conformations agreeing with the predicted structure (Figure 10A,B). This strongest stabilizing mutation simply shortened the side chain by a methyl group, suggesting that the original methyl group made unfavorable interactions. It indeed appears that in the wild type Ile154 is under strain; the dihedral angle among its C, Cα, Cβ, and Cγ1 atoms is an unfavorable −90.4°. The effect of the dihedral angle was modeled using an Amber14 force field (which has clear and separate terms for van der Waals interactions and dihedral energies). Setting said dihedral angle to an ideal −61°, identical with the dihedral angle in the structure of R4 and R6, indeed lowered the dihedral energies ($\Delta E^{\text{dihedral}} = -2$ kJ/(mol subunit)), while the steric clashes increased tremendously ($\Delta E^{\text{van der Waals}} = 7 \times 10^2$ kJ/(mol subunit)). Inspection shows that Ile154 has to adopt the strained dihedral angle to diminish steric clashes with His321′ and Phe323′ (Figure 10C). Thus, a relief of steric strain at the interface can explain the strong stabilizing effect of this subtle mutation. The 3.5-fold increase in catalytic activity by I154V could be due to effects on the tunnel leading to the active site. The I154V mutation causes a shift of 0.6 Å of residue Tyr151 toward Tyr20, decreasing the shape of the active-site entrance tunnel (Figure 10D) with no major backbone changes. These small changes caused by the I154V mutation remodeling the tunnel shape might influence the access of cosolvent or substrates to the active site and influence catalytic activity. Enhanced resistance of a dehalogenase toward cosolvents was also attributed to tunnel mutations by Koudelakova et al.[65]

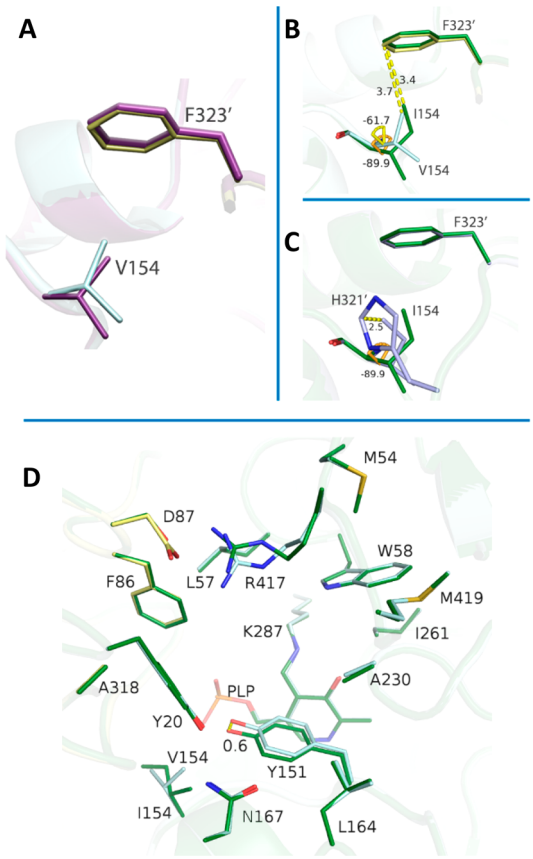

Figure 10. Structural analysis of mutation I154V. (A) Overlay of the R4 crystal structure (chain A in cyan, chain B in yellow) and predicted structure (purple). (B) Comparison of the intersubunit contact (yellow dashed line) between Ile154 and Phe323′ in the wild-type structure (green) and between Val154 and Phe323′ in the R4 crystal structure (cyan, yellow). Dihedral angles are shown for the wild type (orange) and for R4 (yellow), illustrating the elimination of strain by the I154V mutation. (C) Comparison of Ile154 (green) from the wild type against a simulated Ile rotamer (blue) with its ideal dihedral angle, showing how the wild type adopts a strained conformation to reduce steric clashes with His321′ and Phe323′. (D) Comparison of residues forming the active-site entrance tunnel in the wild-type and R4 crystal structures, showing how the I154V mutation causes a slight shift in the position of the Tyr151 side chain. The shift affects the shape of the tunnel leading to the cofactor binding site. Distances are in Å.

Because mutation I154V was also found by the consensus approach, it is less likely that the same substitution can be applied to closely related proteins. Indeed, a valine is already present in the homologous *Ochrobactrum anthropi* TA (PDB 5GHF, 63% sequence identity, Val154),[66] *Vf*TA (4E3Q, 40% identity, Val153), whereas in *Cv*TA (4AH3, 40% identity),[58,67] Ser154 is present at the corresponding position; in all cases the local bond angles do not suggest strain. Furthermore, the subunit interfacial areas of these three TAs are similar, as is apparent from an analysis using PISA[68] (5250, 5300, and 4800 Å^2 for *Pj*TA, *Cv*TA, and *Vf*TA, respectively), whereas it is smaller for *Oa*AT (~4000 Å^2).

The crystal structures thus reveal that the biophysical nature of the stabilizing effects of the designed mutations is diverse. Most of the observed effects are in agreement with known biophysical interactions that contribute to the stability of folded proteins, including mutations stabilizing subunit interfaces.[11] Surprisingly, the largest contribution to enhanced stability is made by substitution I154V, which eliminates strain that is present in the wild-type protein. Enhanced stability by reduced strain is rarely reported, and its discovery by energy calculations and molecular dynamics illustrates the power of computational tools.

CONCLUSIONS

In this work, we used computational design, bioinformatics, and laboratory screening to discover mutations that enhanced the thermostability, cosolvent resistance, IPA compatibility, and catalytic activity of the recently discovered dimeric class III transaminase (TA) from *P. jessenii* (*Pj*TA). The main findings are (1) mutations that stabilize the interface had a much larger positive effect on *Pj*TA stability in comparison to buried or surface mutations and (2) stabilizing mutations at the interface could be predicted with a high success rate with the computational design tools used in the FRESCO workflow. The confirmed individual mutations could be combined and showed cooperative effects, and the final enzymes can be considered thermophilic in view of their optimum temperature.

https://dx.doi.org/10.1021/acscatal.9b05223
ACS Catal. 2020, 10, 2915−2928

The importance of improving interface interactions for better ω-TA stability agrees with observations that inactivation is accompanied by subunit dissociation. Crystal structures of the stabilized *Pj*TA enzymes showed that the mutations can be explained by improved biophysical interactions: additional hydrogen bonding or salt-bridge interactions (S87D/N, E38Q), increased hydrophobic interactions (A60V), introduction of π-stacking (M128F), reduced exposure of hydrophobic surface (P9A), redistribution of electrostatic surface charge (E38Q), and relief of steric strain (I154V).

The stabilizing mutations replace residues that show no high *B* factors in the crystal structures and were mostly not discovered by testing a set of consensus mutations. In general, structures predicted and used by the FoldX and Rosetta energy calculations agreed with the crystal structures, with the exception of Arg417′ in the R6 variant. The use of more stringent energy criteria for selecting mutations did not give a significant increase in the percentage of stabilizing mutations among the selected variants.

The two most robust variants showed increased performance in acetophenone amination reactions, better tolerance to cosolvents, compatibility with high levels of the amino donor (IPA), and improved product yield, while the enantioselectivity was fully retained. The results suggest that the use of this computational workflow to discover stabilizing mutations and optimize subunit interfaces in multimeric enzymes will help to create stable biocatalysts for use in green chemistry.

■ ASSOCIATED CONTENT

Supporting Information

The Supporting Information is available free of charge at https://pubs.acs.org/doi/10.1021/acscatal.9b05223.

Information on all FRESCO and consensus approach mutations, success percentages of the FRESCO libraries generated for eight different enzymes, graphs showing the stability and activities of triple mutants, 4-fold mutants, 5-fold mutants, and 6-fold mutants, and positions of mutations in the structure and along the sequence (PDF)

■ AUTHOR INFORMATION

Corresponding Author

Dick B. Janssen − *Biotransformation and Biocatalysis, Groningen Biomolecular Sciences and Biotechnology Institute (GBB), University of Groningen 9747 AG Groningen, The Netherlands;* orcid.org/0000-0002-0834-2043; Email: d.b.janssen@rug.nl

Authors

Qinglong Meng − *Biotransformation and Biocatalysis, Groningen Biomolecular Sciences and Biotechnology Institute (GBB), University of Groningen 9747 AG Groningen, The Netherlands*

Nikolas Capra − *Biotransformation and Biocatalysis, Groningen Biomolecular Sciences and Biotechnology Institute (GBB), University of Groningen 9747 AG Groningen, The Netherlands*

Cyntia M. Palacio − *Biotransformation and Biocatalysis, Groningen Biomolecular Sciences and Biotechnology Institute (GBB), University of Groningen 9747 AG Groningen, The Netherlands*

Elisa Lanfranchi − *Biotransformation and Biocatalysis, Groningen Biomolecular Sciences and Biotechnology Institute (GBB), University of Groningen 9747 AG Groningen, The Netherlands*

Marleen Otzen − *Biotransformation and Biocatalysis, Groningen Biomolecular Sciences and Biotechnology Institute (GBB), University of Groningen 9747 AG Groningen, The Netherlands*

Luc Z. van Schie − *Biotransformation and Biocatalysis, Groningen Biomolecular Sciences and Biotechnology Institute (GBB), University of Groningen 9747 AG Groningen, The Netherlands*

Henriëtte J. Rozeboom − *Biotransformation and Biocatalysis, Groningen Biomolecular Sciences and Biotechnology Institute (GBB), University of Groningen 9747 AG Groningen, The Netherlands*

Andy-Mark W. H. Thunnissen − *Biotransformation and Biocatalysis, Groningen Biomolecular Sciences and Biotechnology Institute (GBB), University of Groningen 9747 AG Groningen, The Netherlands*

Hein J. Wijma − *Biotransformation and Biocatalysis, Groningen Biomolecular Sciences and Biotechnology Institute (GBB), University of Groningen 9747 AG Groningen, The Netherlands*

Complete contact information is available at: https://pubs.acs.org/10.1021/acscatal.9b05223

Author Contributions

Q.M. and C.M.P. performed the wet-lab experimental work and collected the data. L.Z.v.S. designed and constructed consensus mutants. M.O. and E.L. supported the experimental work and contributed protocols. N.C., H.J.R., and A.-M.W.H.T. solved the crystal structures. H.J.W. and Q.M. designed the mutants. Q.M., N.C., and C.M.P. wrote the manuscript. D.B.J. and H.J.W. revised the manuscript. D.B.J. supervised the project. All authors have given approval to the final version of the manuscript.

Notes

The authors declare no competing financial interest.

■ ACKNOWLEDGMENTS

Q.M. thanks the China Scholarship Council for a Ph.D. fellowship. Part of this project has received funding from the European Union's Horizon 2020 Programme (Marie Curie Actions-ITN ES-Cat) under GA No. 722610, which supported N.C. C.M.P. was supported by Erasmus Mundus, Eurotango II. The work of M.O., E.L., and H.J.W. was supported by the Dutch Ministry of Economic Affairs through BE-Basic, grant FS02.005. We thank the staff of the ESRF at Grenoble for excellent onsite support and beam time allocation.

■ ABBREVIATIONS

TA, transaminase; ATA, amine transaminase; ω-TAs, ω-transaminases; *Cv*TA, TA from *Chromobacterium violaceum*; *Vf*TA, TA from *Vibrio fluvialis*; *Pj*TA, TA from *Pseudomonas jessenii*; PLP, pyridoxal 5′-phosphate; PMP, pyridoxamine 5′-phosphate; T_m^{app}, apparent melting temperature; (*S*)-1-PEA, (*S*)-1-phenylethylamine; IPA, isopropylamine; MSA, multiple sequence alignment

■ REFERENCES

(1) Slabu, I.; Galman, J. L.; Lloyd, R. C.; Turner, N. J. Discovery, Engineering, and Synthetic Application of Transaminase Biocatalysts. *ACS Catal.* **2017**, 7, 8263−8284.

(2) Kelly, S. A.; Pohle, S.; Wharry, S.; Mix, S.; Allen, C. C. R.; Moody, T. S.; Gilmore, B. F. Application of ω-Transaminases in the Pharmaceutical Industry. *Chem. Rev.* **2018**, *118*, 349−367.
(3) Patil, M. D.; Grogan, G.; Bommarius, A.; Yun, H. Recent Advances in ω-Transaminase-Mediated Biocatalysis for the Enantioselective Synthesis of Chiral Amines. *Catalysts* **2018**, *8*, 254.
(4) Eliot, A. C.; Kirsch, J. F. Pyridoxal Phosphate Enzymes: Mechanistic, Structural, and Evolutionary Considerations. *Annu. Rev. Biochem.* **2004**, *73*, 383−415.
(5) Stepankova, V.; Bidmanova, S.; Koudelakova, T.; Prokop, Z.; Chaloupkova, R.; Damborsky, J. Strategies for Stabilization of Enzymes in Organic Solvents. *ACS Catal.* **2013**, *3*, 2823−2836.
(6) Bornscheuer, U. T.; Huisman, G. W.; Kazlauskas, R. J.; Lutz, S.; Moore, J. C.; Robins, K. Engineering the Third Wave of Biocatalysis. *Nature* **2012**, *485*, 185−194.
(7) Schiroli, D.; Peracchi, A. A Subfamily of PLP-Dependent Enzymes Specialized in Handling Terminal Amines. *Biochim. Biophys. Acta, Proteins Proteomics* **2015**, *1854*, 1200−1211.
(8) Börner, T.; Rämisch, S.; Bartsch, S.; Vogel, A.; Adlercreutz, P.; Grey, C. Three in One: Temperature, Solvent and Catalytic Stability by Engineering the Cofactor-Binding Element of Amine Transaminase. *ChemBioChem* **2017**, *18*, 1482−1486.
(9) Börner, T.; Rämisch, S.; Reddem, E. R.; Bartsch, S.; Vogel, A.; Thunnissen, A-M. W. H.; Adlercreutz, P.; Grey, C. Explaining Operational Instability of Amine Transaminases: Substrate-Induced Inactivation Mechanism and Influence of Quaternary Structure on Enzyme-Cofactor Intermediate Stability. *ACS Catal.* **2017**, *7*, 1259−1269.
(10) Chen, S.; Berglund, P.; Humble, M. S. The Effect of Phosphate Group Binding Cup Coordination on the Stability of the Amine Transaminase from *Chromobacterium violaceum*. *Mol. Catal.* **2018**, *446*, 115−123.
(11) Fernandez-Lafuente, R. Stabilization of Multimeric Enzymes: Strategies to Prevent Subunit Dissociation. *Enzyme Microb. Technol.* **2009**, *45*, 405−418.
(12) Palacio, C. M.; Rozeboom, H. J.; Lanfranchi, E.; Meng, Q.; Otzen, M.; Janssen, D. B. Biochemical Properties of a *Pseudomonas* Aminotransferase Involved in Caprolactam Metabolism. *FEBS J.* **2019**, *286*, 4086−4102.
(13) Das, R.; Baker, D. Macromolecular Modeling with Rosetta. *Annu. Rev. Biochem.* **2008**, *77*, 363−382.
(14) Richter, F.; Leaver-Fay, A.; Khare, S. D.; Bjelic, S.; Baker, D. De Novo Enzyme Design using Rosetta3. *PLoS One* **2011**, *6*, No. e19230.
(15) Goldenzweig, A.; Fleishman, S. J. Principles of Protein Stability and Their Application in Computational Design. *Annu. Rev. Biochem.* **2018**, *87*, 105−129.
(16) Musil, M.; Konegger, H.; Hon, J.; Bednar, D.; Damborsky, J. Computational Design of Stable and Soluble Biocatalysts. *ACS Catal.* **2019**, *9*, 1033−1054.
(17) Eijsink, V. G.; Bjørk, A.; Gåseidnes, S.; Sirevåg, R.; Synstad, B.; van den Burg, B.; Vriend, G. Rational Engineering of Enzyme Stability. *J. Biotechnol.* **2004**, *113*, 105−120.
(18) Korkegian, A.; Black, M. E.; Baker, D.; Stoddard, B. L. Computational Thermostabilization of an Enzyme. *Science* **2005**, *308*, 857−860.
(19) Schweiker, K. L.; Makhatadze, G. I. Protein Stabilization by the Rational Design of Surface Charge-Charge Interactions. *Methods Mol. Biol.* **2009**, *490*, 261−283.
(20) Gribenko, A. V.; Patel, M. M.; Liu, J.; McCallum, S. A.; Wang, C.; Makhatadze, G. I. Rational Stabilization of Enzymes by Computational Redesign of Surface Charge-Charge Interactions. *Proc. Natl. Acad. Sci. U. S. A.* **2009**, *106*, 2601−2606.
(21) Lee, C. W.; Wang, H. J.; Hwang, J. K.; Tseng, C. P. Protein Thermal Stability Enhancement by Designing Salt Bridges: A Combined Computational and Experimental Study. *PLoS One* **2014**, *9*, No. e112751.
(22) Pikkemaat, M. G.; Linssen, A. B.; Berendsen, H. J.; Janssen, D. B. Molecular Dynamics Simulations as a Tool for Improving Protein Stability. *Protein Eng., Des. Sel.* **2002**, *15*, 185−192.
(23) Porebski, B. T.; Buckle, A. M. Consensus Protein Design. *Protein Eng., Des. Sel.* **2016**, *29*, 245−251.
(24) Lehmann, M.; Kostrewa, D.; Wyss, M.; Brugger, R.; D'Arcy, A.; Pasamontes, L.; van Loon, A. P. From DNA Sequence to Improved Functionality: Using Protein Sequence Comparisons to Rapidly Design a Thermostable Consensus Phytase. *Protein Eng., Des. Sel.* **2000**, *13*, 49−57.
(25) Lehmann, M.; Loch, C.; Middendorf, A.; Studer, D.; Lassen, S. F.; Pasamontes, L.; van Loon, A. P.; Wyss, M. The Consensus Concept for Thermostability Engineering of Proteins: Further Proof of Concept. *Protein Eng., Des. Sel.* **2002**, *15*, 403−411.
(26) Bednar, D.; Beerens, K.; Sebestova, E.; Bendl, J.; Khare, S.; Chaloupkova, R.; Prokop, Z.; Brezovsky, J.; Baker, D.; Damborsky, J. FireProt: Energy- and Evolution-Based Computational Design of Thermostable Multiple-Point Mutants. *PLoS Comput. Biol.* **2015**, *11*, No. e1004556.
(27) Goldenzweig, A.; Goldsmith, M.; Hill, S. E.; Gertman, O.; Laurino, P.; Ashani, Y.; Dym, O.; Unger, T.; Albeck, S.; Prilusky, J.; Lieberman, R. L.; Aharoni, A.; Silman, I.; Tawfik, D. S.; Fleishman, S. J. Automated Structure- and Sequence-Based Design of Proteins for High Bacterial Expression and Stability. *Mol. Cell* **2016**, *63*, 337−346.
(28) Vázquez-Figueroa, E.; Chaparro-Riggers, J.; Bommarius, A. S. Development of a thermostable glucose dehydrogenase by a structure-guided consensus concept. *ChemBioChem* **2007**, *8*, 2295−2301.
(29) Bosshart, A.; Panke, S.; Bechtold, M. Systematic Optimization of Interface Interactions Increases the Thermostability of a Multimeric Enzyme. *Angew. Chem., Int. Ed.* **2013**, *52*, 9673−9676.
(30) Wijma, H. J.; Floor, R. J.; Jekel, P. A.; Baker, D.; Marrink, S. J.; Janssen, D. B. Computationally Designed Libraries for Rapid Enzyme Stabilization. *Protein Eng., Des. Sel.* **2014**, *27*, 49−58.
(31) Floor, R. J.; Wijma, H. J.; Colpa, D. I.; Ramos-Silva, A.; Jekel, P. A.; Szymański, W.; Feringa, B. L.; Marrink, S. J.; Janssen, D. B. Computational Library Design for Increasing Haloalkane Dehalogenase Stability. *ChemBioChem* **2014**, *15*, 1660−1672.
(32) Wu, B.; Wijma, H. J.; Song, L.; Rozeboom, H. J.; Poloni, C.; Tian, Y.; Arif, M. I.; Nuijens, T.; Quaedflieg, P. J. L. M.; Szymanski, W.; Feringa, B. L.; Janssen, D. B. Versatile Peptide C-Terminal Functionalization via a Computationally Engineered Peptide Amidase. *ACS Catal.* **2016**, *6*, 5405−5414.
(33) Bu, Y.; Cui, Y.; Peng, Y.; Hu, M.; Tian, Y.; Tao, Y.; Wu, B. Engineering Improved Thermostability of the GH11 Xylanase from *Neocallimastix patriciarum* via Computational Library Design. *Appl. Microbiol. Biotechnol.* **2018**, *102*, 3675−3685.
(34) Martin, C.; Ovalle Maqueo, A.; Wijma, H. J.; Fraaije, M. W. Creating a More Robust 5-Hydroxymethylfurfural Oxidase by Combining Computational Predictions with a Novel Effective Library Design. *Biotechnol. Biofuels* **2018**, *11*, 56.
(35) Fürst, M. J. L. J.; Boonstra, M.; Bandstra, S.; Fraaije, M. W. Stabilization of Cyclohexanone Monooxygenase by Computational and Experimental Library Design. *Biotechnol. Bioeng.* **2019**, *116*, 2167−2177.
(36) Arabnejad, H.; Dal Lago, M.; Jekel, P. A.; Floor, R. J.; Thunnissen, A-M. W. H.; Terwisscha van Scheltinga, A. C.; Wijma, H. J.; Janssen, D. B. A Robust Cosolvent-Compatible Halohydrin Dehalogenase by Computational Library Design. *Protein Eng., Des. Sel.* **2016**, *30*, 173−187.
(37) Wijma, H. J.; Fürst, M. J. L. J.; Janssen, D. B. A Computational Library Design Protocol for Rapid Improvement of Protein Stability: FRESCO. *Methods Mol. Biol.* **2018**, *1685*, 69−85.
(38) Kellogg, E. H.; Leaver-Fay, A.; Baker, D. Role of Conformational Sampling in Computing Mutation-Induced Changes in Protein Structure and Stability. *Proteins: Struct., Funct., Genet.* **2011**, *79*, 830−838.
(39) Guerois, R.; Nielsen, J. E.; Serrano, L. Predicting Changes in the Stability of Proteins and Protein Complexes: A Study of More than 1000 Mutations. *J. Mol. Biol.* **2002**, *320*, 369−387.
(40) Krieger, E.; Darden, T.; Nabuurs, S. B.; Finkelstein, A.; Vriend, G. Making Optimal Use of Empirical Energy Functions: Force-Field

https://dx.doi.org/10.1021/acscatal.9b05223
ACS Catal. 2020, 10, 2915−2928

Parameterization in Crystal Space. *Proteins: Struct., Funct., Genet.* **2004**, *57*, 678−683.
(41) Ashkenazy, H.; Abadi, S.; Martz, E.; Chay, O.; Mayrose, I.; Pupko, T.; Ben-Tal, N. ConSurf 2016: an Improved Methodology to Estimate and Visualize Evolutionary Conservation in Macromolecules. *Nucleic Acids Res.* **2016**, *44*, W344−W350.
(42) Reetz, M. T.; Carballeira, J. D.; Vogel, A. Iterative Saturation Mutagenesis on the Basis of B Factors as a Strategy for Increasing Protein Thermostability. *Angew. Chem., Int. Ed.* **2006**, *45*, 7745−7751.
(43) Reetz, M. T.; Soni, P.; Fernández, L.; Gumulya, Y.; Carballeira, J. D. Increasing the Stability of an Enzyme Toward Hostile Organic Solvents by Directed Evolution Based on Iterative Saturation Mutagenesis Using the B-FIT Method. *Chem. Commun. (Cambridge, U. K.)* **2010**, *46*, 8657−8658.
(44) Krieger, E.; Vriend, G. YASARA View - Molecular Graphics for all Devices - from Smartphones to Workstations. *Bioinformatics* **2014**, *30*, 2981−2982.
(45) Maier, J. A.; Martinez, C.; Kasavajhala, K.; Wickstrom, L.; Hauser, K. E.; Simmerling, C. ff14SB: Improving the Accuracy of Protein Side Chain and Backbone Parameters from ff99SB. *J. Chem. Theory Comput.* **2015**, *11*, 3696−3713.
(46) Ericsson, U. B.; Hallberg, B. M.; DeTitta, G. T.; Dekker, N.; Nordlund, P. Thermofluor-Based High-Throughput Stability Optimization of Proteins for Structural Studies. *Anal. Biochem.* **2006**, *357*, 289−298.
(47) Boivin, S.; Kozak, S.; Meijers, R. Optimization of Protein Purification and Characterization Using Thermofluor Screens. *Protein Expression Purif.* **2013**, *91*, 192−206.
(48) Schätzle, S.; Höhne, M.; Redestad, E.; Robins, K.; Bornscheuer, U. T. Rapid and Sensitive Kinetic Assay for Characterization of ω-Transaminases. *Anal. Chem.* **2009**, *81*, 8244−8248.
(49) Mathew, S.; Nadarajan, S. P.; Chung, T.; Park, H. H.; Yun, H. Biochemical Characterization of Thermostable ω-Transaminase from *Sphaerobacter thermophilus* and Its Application for Producing Aromatic β- and γ-Amino Acids. *Enzyme Microb. Technol.* **2016**, *87*−*88*, 52−60.
(50) Battye, T. G.; Kontogiannis, L.; Johnson, O.; Powell, H. R.; Leslie, A. G. iMOSFLM: a New Graphical Interface for Diffraction-Image Processing with MOSFLM. *Acta Crystallogr., Sect. D: Biol. Crystallogr.* **2011**, *67*, 271−281.
(51) Kabsch, W. XDS. *Acta Crystallogr., Sect. D: Biol. Crystallogr.* **2010**, *D66*, 125−132.
(52) Evans, P. R.; Murshudov, G. N. How Good are my Data and What is the Resolution? *Acta Crystallogr., Sect. D: Biol. Crystallogr.* **2013**, *D69*, 1204−1214.
(53) Winn, M. D.; Ballard, C. C.; Cowtan, K. D.; Dodson, E. J.; Emsley, P.; Evans, P. R.; Keegan, R. M.; Krissinel, E. B.; Leslie, A. G.; McCoy, A.; McNicholas, S. J.; Murshudov, G. N.; Pannu, N. S.; Potterton, E. A.; Powell, H. R.; Read, R. J.; Vagin, A.; Wilson, K. S. Overview of the CCP4 Suite and Current Developments. *Acta Crystallogr., Sect. D: Biol. Crystallogr.* **2011**, *D67*, 235−242.
(54) Murshudov, G. N.; Vagin, A. A.; Dodson, E. J. Refinement of Macromolecular Structures by the Maximum-Likelihood Method. *Acta Crystallogr., Sect. D: Biol. Crystallogr.* **1997**, *D53*, 240−255.
(55) Emsley, P.; Lohkamp, B.; Scott, W. G.; Cowtan, K. Features and Development of Coot. *Acta Crystallogr., Sect. D: Biol. Crystallogr.* **2010**, *D66*, 486−501.
(56) *The PyMOL Molecular Graphics System, ver. 2.1.0*; Schrödinger, LLC.
(57) Buss, O.; Muller, D.; Jager, S.; Rudat, J.; Rabe, K. S. Improvement in the Thermostability of a β-Amino Acid Converting ω-Transaminase by Using FoldX. *ChemBioChem* **2018**, *19*, 379−387.
(58) Land, H.; Campillo-Brocal, J. C.; Svedendahl Humble, M.; Berglund, P. B-factor Guided Proline Substitutions in *Chromobacterium violaceum* Amine Transaminase: Evaluation of the Proline Rule as a Method for Enzyme Stabilization. *ChemBioChem* **2019**, *20*, 1297−1304.
(59) Wang, X.; Lin, H.; Zheng, Y.; Feng, J.; Yang, Z.; Tang, L. MDC-Analyzer-Facilitated Combinatorial Strategy for Improving the Activity and Stability of Halohydrin Dehalogenase from *Agrobacterium radiobacter* AD1. *J. Biotechnol.* **2015**, *206*, 1−7.
(60) Mathew, S.; Deepankumar, K.; Shin, G.; Hong, E. Y.; Kim, B.-G.; Chung, T.; Yun, H. Identification of Novel Thermostable ω-Transaminase and Its Application for Enzymatic Synthesis of Chiral Amines at High Temperature. *RSC Adv.* **2016**, *6*, 69257−69260.
(61) Park, E. S.; Dong, J. Y.; Shin, J. S. ω-Transaminase-Catalyzed Asymmetric Synthesis of Unnatural Amino Acids Using Isopropylamine as an Amino Donor. *Org. Biomol. Chem.* **2013**, *11*, 6929−6933.
(62) Kelefiotis-Stratidakis, P.; Tyrikos-Ergas, T.; Pavlidis, I. V. The Challenge of Using Isopropylamine as an Amine Donor in Transaminase Catalysed Reactions. *Org. Biomol. Chem.* **2019**, *17*, 1634−1642.
(63) Dawood, A. W. H.; Weiß, M. S.; Schulz, C.; Pavlidis, I. V.; Iding, H.; de Souza, R. O. M. A.; Bornscheuer, U. T. Isopropylamine as Amine Donor in Transaminase-Catalyzed Reactions: Better Acceptance through Reaction and Enzyme Engineering. *ChemCatChem* **2018**, *10*, 3943−3949.
(64) Hirotsu, K.; Goto, M.; Okamoto, A.; Miyahara, I. Dual Substrate Recognition of Aminotransferases. *Chem. Rec.* **2005**, *5*, 160−172.
(65) Koudelakova, T.; Chaloupkova, R.; Brezovsky, J.; Prokop, Z.; Sebestova, E.; Hesseler, M.; Khabiri, M.; Plevaka, M.; Kulik, D.; Kuta-Smatanova, I.; Rezacova, P.; Ettrich, R.; Bornscheuer, U. T.; Damborsky, J. Engineering Enzyme Stability and Resistance to an Organic Cosolvent by Modification of Residues in the Access Tunnel. *Angew. Chem., Int. Ed.* **2013**, *52*, 1959−1963.
(66) Han, S.-W.; Kim, J.; Cho, H.-S.; Shin, J.-S. Active Site Engineering of Omega-Transaminase Guided by Docking Orientation Analysis and Virtual Activity Screening. *ACS Catal.* **2017**, *7*, 3752−3762.
(67) Kaulmann, U.; Smithies, K.; Smith, M. E. B.; Hailes, H. C.; Ward, J. M. Substrate Spectrum of ω-Transaminase from *Chromobacterium violaceum* DSM30191 and its Potential for Biocatalysis. *Enzyme Microb. Technol.* **2007**, *41*, 628−637.
(68) Krissinel, E.; Henrick, K. Inference of Macromolecular Assemblies from Crystalline State. *J. Mol. Biol.* **2007**, *372*, 774−797.

https://dx.doi.org/10.1021/acscatal.9b05223
ACS Catal. 2020, 10, 2915−2928